# Localization of dynein light chains 1 and 2 and their pro-apoptotic ligands

Catherine L. DAY*, Hamsa PUTHALAKATH†, Gretchen SKEA*, Andreas STRASSER†, Igor BARSUKOV‡, Lu-Yun LIAN§, David C. S. HUANG† and Mark G. HINDS†[1]

*Department of Biochemistry, University of Otago, Dunedin, New Zealand, †The Walter and Eliza Hall Institute of Medical Research, 1G Royal Parade, Parkville, VIC 3050, Australia, ‡Biological NMR Centre, University of Leicester, Leicester, U.K., and §Department of Biomolecular Sciences, UMIST, Manchester, U.K.

The dynein and myosin V motor complexes are multi-protein structures that function to transport molecules and organelles within the cell. DLC (dynein light-chain) proteins, found as components of both dynein and myosin V motor complexes, connect the complexes to their cargoes. One of the roles of these motor complexes is to selectively sequester the pro-apoptotic 'BH3-only' (Bcl-2 homology 3-only) proteins, Bim (Bcl-2-interacting mediator of cell death) and Bmf (Bcl-2-modifying factor), and so regulate their cell death-inducing function. *In vivo* DLC2 is found exclusively as a component of the myosin V motor complex and Bmf binds DLC2 selectively. On the other hand, Bim interacts with DLC1 (LC8), an integral component of the dynein motor complex. The two DLCs share 93 % sequence identity yet show unambiguous *in vivo* specificity for their respective BH3-only ligands. To investigate this specificity the three-dimensional solution structure of DLC2 was elucidated using NMR spectroscopy. *In vitro* structural and mutagenesis studies show that Bmf and Bim have identical binding characteristics to recombinant DLC2 or DLC1. Thus the selectivity shown by Bmf and Bim for binding DLC1 or DLC2, respectively, does not reside in their DLC-binding domains. Remarkably, mutational analysis of DLC1 and DLC2 indicates that a single surface residue (residue 41) determines the specific localization of DLCs with their respective motor complexes. These results suggest a molecular mechanism for the specific compartmentalization of DLCs and their pro-apoptotic cargoes and implicate other protein(s) in defining the specificity between the cargoes and the DLC proteins.

Key words: apoptosis, Bcl-2 homology 3-only protein (BH3-only protein), dynein light chain, localization, NMR, structure.

## INTRODUCTION

Pro-apoptotic Bcl-2 family proteins, particularly the 'BH3-only' (Bcl-2 homology 3-only) members, are essential inducers of programmed cell death and stress-induced apoptosis [1–3]. In mammals, eight BH3-only proteins, including Bik/Blk/Nbk, Puma/Bbc3, Noxa, Bim (Bcl-2-interacting mediator of cell death)/Bod, Bid, Hrk/DP5, Bad and Bmf (Bcl-2-modifying factor), have been identified [3,4]. These molecules share a short BH3 domain required for binding their cognate pro-survival Bcl-2 partners. Strict regulation of these proteins is essential to rein in their potent cell death-inducing capacity. A multiplicity of mechanisms has evolved to keep these molecules in check. For example, Hrk, Noxa and Puma [5–7] are transcriptionally regulated whereas Bad, Bid, Bim and Bmf are predominantly subject to post-translational controls that include phosphorylation (Bad), enzymic cleavage (Bid) and sequestration (Bim, Bmf), or a combination of these methods. In general, these pro-apoptotic proteins are kept inert and primed to sense distinct forms of cellular stress. Once activated, the BH3-only proteins are released to trigger apoptosis by binding to pro-survival Bcl-2 proteins. Since the BH3-only proteins are critical initiators of apoptosis, understanding how they function at the atomic level is a key step in elucidating the molecular events that lead to apoptosis. Of particular interest are the specificities of interactions between the BH3-only proteins and their cognate regulators.

Bim [8] and Bmf [9] are two pro-apoptotic BH3-only proteins that signal to the cell death machinery by sensing cellular damage that affects the cell cytoskeleton. In healthy cells both Bim and Bmf are sequestered away from the sites where pro-survival Bcl-2 family members reside (cytoplasmic face of the nuclear, endoplasmic reticulum and mitochondria membranes), through interaction with DLC (dynein light-chain) proteins. The light chains have a molecular mass less than approx. 22 kDa, associate with the intermediate chains, and are integral components of motor complexes. There are three molecular mass ranges for the light chains, approx. 8, 14 and 22 kDa, and the 8 kDa family are referred to as either light chains or DLC and bind proteins such as Bim and Bmf. Specifically, the light-chain component of the myosin V motor complex, known as DLC2, binds Bmf, while the equivalent component of cytoplasmic dynein known as either DLC1, LC8, cytoplasmic DLC or PIN [protein inhibitor of nNOS (neuronal nitric oxide synthase)] [10], referred to here as DLC1, binds Bim in healthy cells. In response to apoptotic stimuli that impact upon the motor complexes, Bim or Bmf, in complex with their respective light chains, are released into the cytoplasm where they can interact with pro-survival Bcl-2 proteins, via their BH3 domains [11].

Interaction of Bim and Bmf with the DLCs appears to have a critical role in regulating their pro-apoptotic activites. Mutations in the LBD (light-chain-binding domain) of Bim or Bmf, that disrupt binding to the respective DLCs [8,9], enhance the death-promoting activity of these proteins, and cells expressing such mutant proteins are considerably more susceptible to death stimuli than those expressing their wild-type counterparts. Furthermore, analysis of the three Bim splice variants, $Bim_{EL}$, $Bim_{L}$ and $Bim_{S}$, also suggests an important regulatory role for DLC interaction. $Bim_{S}$, which lacks the LBD-containing exon present in the longer Bim isoforms, is the most potent apoptosis inducer, probably because it is not restrained through interaction with DLC1 [8]. Phosphorylation of residues in the LBD of Bim and Bmf may also regulate the release of these molecules from their motor complexes [12].

Abbreviations used: Bim, Bcl-2-interacting mediator of cell death; BH3, Bcl-2 homology 3; Bmf, Bcl-2-modifying factor; DLC, dynein light chain; HSQC, heteronuclear single-quantum coherence spectroscopy; nNOS, neuronal nitric oxide synthase; rmsd, root mean square deviation; LBD, light chain-binding domain; GST, glutathione S-transferase; 3D, three-dimensional; NOESY, nuclear Overhauser enhancement spectroscopy; NOE, nuclear Overhauser effect.

[1] To whom correspondence should be addressed (e-mail mhinds@wehi.edu.au).

The highly conserved homodimeric DLCs function to tether their payloads on to the motor complexes for transport along either actin filaments or microtubules. Many cargoes have been reported to bind DLCs, including cellular proteins [13,14], mRNA [15], organelles [16], viral proteins [17,18] and particles [19]. A combination of biochemical and mutational studies has identified a conserved (K/R)XTQT consensus sequence within these proteins that is required for binding DLC1 [8,13]. This motif is found in both Bim and Bmf. A second sequence motif, G(I/V)QV(D/E), was identified by a peptide-scanning approach seeking DLC-targeted proteins [14].

Three-dimensional structures have been determined for DLC1 alone [20,21], and in complex with peptide fragments from nNOS [22] and from $Bim_L$ [21]. The crystal structure of DLC1 bound to a 13-residue peptide fragment from nNOS showed that the peptide-binding site is a deep hydrophobic cleft formed by strands $\beta3$, $\beta4$ and $\beta5$ from one protomer and $\alpha2$ from the other. The peptide interacts extensively, via backbone hydrogen bonds, and side-chain hydrophobic and hydrophilic interactions, with strand $\beta3$ in an anti-parallel manner, extending the central $\beta$-sheet of DLC1 to six anti-parallel $\beta$-strands. The ligand specificity of DLC1 is determined by a combination of main-chain and side-chain hydrogen bonds, together with the steric complementarity between the ligand and DLC1. In summary, structural and mutagenesis studies have provided the molecular basis for the binding specificity of the LBD recognition sequence to DLC1 [22].

Whereas the interactions between Bim and DLC1 have been investigated in detail, less is known about the interaction between Bmf and DLC2. Significantly, it is unknown as to why, *in vivo*, Bmf binds specifically to DLC2. We report here the structure of DLC2, and compare the binding of DLC2 and DLC1 to both Bim and Bmf peptides. In addition, the specific localization of Bim and Bmf was probed using both *in vitro* experiments to define, if any, the specificity between the light chains and the BH3-only proteins; and *in vivo* experiments involving transfection of mammalian cells with wild-type and mutant DLCs to determine the specificities with the motor complexes.

Our data show that binding of Bmf to DLC2 is similar to $Bim_L$ binding to DLC1 and that the recombinant C-terminally truncated Bim and Bmf proteins bind both the DLCs with equal avidity. Hence, the *in vivo* specificity of Bmf for DLC2 must be due to other as-yet-unidentified molecules influencing the formation of the Bmf–DLC2 complex. We also show that unlike the promiscuous interactions between Bim or Bmf and DLC1 or DLC2, the specific interactions of DLC1 with the dynein V motor complex, and of DLC2 with the myosin V motor complex, appear to be largely mediated by residue 41 of the DLCs.

## EXPERIMENTAL

### Protein expression and purification

Murine DLC1, DLC2, C-terminally truncated $Bim_L\Delta C27$ ($Bim_L$ truncated by 27 residues) and $Bmf\Delta C25$ (Bmf truncated by 25 residues) were expressed as GST (glutathione S-transferase) fusion proteins in *Escherichia coli* BL21 (DE3) using established protocols [23]. Proteins were purified by affinity chromatography using glutathione–Sepharose (Amersham Biosciences), cleaved with PreScission protease (Amersham Biosciences) and further purified by size-exclusion chromatography using Superdex 75 (Amersham Biosciences). DLC1 prepared by this method contained two additional vector-derived N-terminal residues (GS) while DLC2 had five additional N-terminal residues (GPLGS). Isotopically labelled proteins were prepared as described previously [23]. NMR samples contained approx. 1 mM protein in 50 mM sodium phosphate (pH 6.7), 70 mM NaCl, 2 mM TCEP [Tris-(carboxyethyl) phosphine hydrochloride] and 0.04 % sodium azide in $H_2O/^2H_2O$ (95:5 v/v). Site-specific mutants of $Bim_L$, Bmf and DLC were generated using a PCR-based strategy as described previously [23]. The sequence of all clones was confirmed by DNA sequencing.

Peptides corresponding to the LBDs of mouse Bmf (residues 64–80, SQEDKATQTLSPASPSQ) and mouse $Bim_L$ (residues 48–64, MSCDKSTQTPSPPCQAF) were purchased from Auspep. Peptide purity was confirmed by electrospray MS. DLC1– or DLC2–peptide complexes were formed by addition of equimolar solutions of LBD peptide to DLC protein and the mixture concentrated to a final protein concentration of approx. 1 mM.

### Binding studies

Direct interactions between DLC1 or DLC2 and $Bim_L$ or Bmf were monitored using GST pull-down experiments. These were performed in 100 $\mu$l of PBS (pH 7.3) containing 2 mM dithiothreitol. Typically, excess soluble protein was then added to equivalent amounts of resin-bound protein. After incubation at room temperature for 30 min the resin was pelleted, washed twice with 200 $\mu$l of PBS containing 0.2 % Tween 20 and 10 $\mu$l of $2\times$ SDS sample buffer was added to each sample. The samples were boiled, loaded on to 16 % acrylamide gels, electrophoresed and then stained with Coomassie Blue. The staining intensity of the bound soluble protein indicated the strength of the interaction between the two proteins.

### Yeast reverse two-hybrid screens

To identify the DLC1 residues required for $Bim_L$ binding, a yeast reverse two-hybrid screen was undertaken as outlined by our earlier studies [8]. Random mutations of DLC1 were subcloned into pGAD 424 EGFP and the clones were screened for loss of binding to $Bim_L$, as indicated by growth in 0.2 % 5-fluoro-orotic acid. Non-interacting clones were viable. To confirm this, a $\beta$-galactosidase assay was performed [8,9,24]. The plasmids that encode non-interacting DLC1 clones were rescued and sequenced [9,25].

### NMR spectroscopy and spectral assignments

A series of two-dimensional and 3D (three-dimensional) heteronuclear NMR spectra were acquired on free DLC1 or that bound to $Bim_L$-LBD, and free DLC2 or that bound to Bmf-LBD, at 25 °C on a Bruker DRX 600 spectrometer equipped with triple-resonance pulsed-field gradient probe. Sequential resonance assignments of unbound DLC2 and the complexes of DLC1 studied here were made, in part, by comparison with those of DLC1 and its complex with nNOS (I. Barsukov and L.-Y. Lian, unpublished work). Additional experiments using a series of triple resonance spectra were acquired on either uniformly $^{15}N$-labelled or $^{13}C$-/$^{15}N$-labelled protein [26]. Exchange properties of the HN protons were monitored by CLEANEX-PM HSQC (heteronuclear single-quantum coherence spectroscopy) spectra [27]. $^{15}N$-DLC1 and $^{15}N$-DLC2 were titrated with aliquots of Bim and Bmf peptides. Spectra were processed using XWIN-NMR (Bruker AG) and analysed using XEASY [28].

### Structure calculation

Approximate inter-proton distances were derived from two-dimensional NOESY (nuclear Overhauser enhancement

spectroscopy) and 3D $^{13}C$- and $^{15}N$-edited NOESY spectra with 150 ms mixing times. Backbone-$\varphi$ constraints were determined from $^{3}J_{HNHA}$ coupling constants obtained from a HNHA spectrum. $\psi$ angles were restricted according to the value of the chemical shift of their C$\alpha$ resonance [29]. Remaining residues were restricted in their $\varphi$ angle according to Luginbühl et al. [29] or to negative $\varphi$ angles where the condition for a positive $\varphi$ angle was not met [30]. A positive $\varphi$ angle for residue Asp-51 was characterized by both an intense intra-residue H$\alpha$-HN NOE (nuclear Overhauser effect) and a weak sequential H$\alpha$-HN NOE in conjunction with a $^{3}J_{HNHA}$ coupling constant of 6 Hz. The $\varphi$ angle of residue Asp-51 was restricted to a range of $60 \pm 30°$ in the structure calculation [30]. Hydrogen-bond constraints were applied at a late stage of the structure calculation where there existed the characteristic NOE patterns observed for $\alpha$-helices or $\beta$-strands and slow-exchanging HN protons [23].

A total of 99 inter-protomer distance constraints were applied for the calculation of the dimer; these constraints were classified as being between the protomers as they could not be satisfied in a monomer structure alone. The dimer structure was calculated according to the protocols of O'Donoghue et al. [31] for determining structures of symmetrical multimeric proteins. Briefly, the crystal structure of DLC1 (PDB code 1CMI) [22] was used as a guide in the location of cross-protomer NOEs in DLC2. Two symmetrically arranged protomers were generated by duplication and rotation of the monomer structure to form an initial dimer that satisfied the inter-protomer distance restraints. Further constraint was applied in the form of non-crystallographic symmetry restraints to maintain the 2-fold symmetry of the molecule [31]. Initial structure calculations were performed using DYANA [32] and once the final set of restraints had been obtained a new family of structures was refined using CNS (1.0) [33]. Non-crystallographic symmetry restraints were applied to residues 5–89 to maintain the dimer symmetry. Structures with the lowest penalty function were minimized using the OPLSX non-bonded parameters [34] while maintaining the 2-fold symmetry. Structural analysis was performed on the 20 structures with the lowest stereochemical energies and PROCHECK_NMR [35] was used for assessment of their stereochemical quality. The structures had no experimental distance violations greater than 0.3 Å or dihedral angle violations greater than 5°. Structural figures were created using MOLMOL [36]. The atomic co-ordinates have been deposited in the Protein Data Bank, Research Collaboratory for Structural Bioinformatics, Rutgers University, New Brunswick, NJ, U.S.A. (http://www.rcsb.org), under PDB code 1RE6.

### Mammalian expression vectors, transient transfection and subcellular fractionation

Mammalian expression vectors for DLC1 and DLC2 have been described previously [8,9], as has liposome-mediated transient transfection of HEK-293T cells [37,38]. Mutants of DLC1 and DLC2 were generated by PCR using proofreading *Pfu* polymerase (Stratagene) and the constructs verified by automated sequencing. Details of the oligonucleotides and the constructs are available from the authors.

Equivalent cell numbers from parental or transiently transfected HEK-293T cells were lysed in 500 $\mu$l of extraction buffer [0.05 M Pipes/NaOH, 0.05 M Hepes, pH 7.0, 2 mM $MgCl_2$, 1 mM EDTA, protease inhibitors (Complete™ tablets; Roche) and 1 % Triton X-100] on ice for 30 min. Cellular debris was removed by centrifugation (10 000 ***g***, 4 °C) and the resultant supernatant was centrifuged at 125 000 ***g*** for 1 h at 4 °C in a Beckman bench-top ultracentrifuge. The pellet (P1) is enriched for the myosin V motor [39]. Paclitaxel (final concentration, 20 $\mu$M; Taxol, Sigma) and 4 units of apyrase (Sigma) were added to the remaining supernatant, which was incubated at 37 °C for 12 min with occasional swirling. This extract was then loaded on to a 7.5 % sucrose cushion made in the extraction buffer (500 $\mu$l of cushion, prewarmed to 37 °C) and spun at 125 000 ***g*** for 1 h at 30 °C. The microtubule-enriched pellet was saved as P2 [40]. Pellets P1 and P2 were boiled in SDS sample buffer before electrophoresis.

### Antibodies

The antibodies used in this study are mouse monoclonal antibodies anti-FLAG M2 (Sigma) and anti-(dynein intermediate chain 74) (IC74) clone 70.1 (Sigma), and rabbit polyclonal antibody anti-myosin V (a gift from Professor R. Cheney, University of North Carolina at Chapel Hill, NC, U.S.A.).

## RESULTS

### Solution structure of the DLC2 dimer

Almost complete, sequence-specific, backbone and side-chain assignments for the $^{1}H$, $^{13}C$ and $^{15}N$ resonances of double-labelled DLC2 were determined using a series of heteronuclear 3D NMR methods [26]. Structures were calculated using earlier protocols [23]. The parameters characterizing the final 20 structures, and structural statistics summarized in Table 1, demonstrate that the ensemble of NMR structures is energetically reasonable and has acceptable covalent geometry. Figure 1(A) shows the superposition of the final structures over the backbone atoms (N, C$\alpha$, C′) of residues 5–89 and 5′–89′ of the dimer.

The 3D structure of the DLC2 monomer subunit comprises a short N-terminal strand followed by two helices ($\alpha$1, $\alpha$2) that are connected by a tight turn (Figure 1B). These helices are packed against a five-stranded $\beta$-sheet that is formed by the N-terminal strand and four additional strands, one of which is derived from the adjacent monomer. Close contacts between residues of $\beta$2, the second $\beta$ strand of one subunit, and $\beta$3′, the third strand of the adjacent subunit, extends the $\beta$-sheet formed by strands $\beta$1, $\beta$2, $\beta$4 and $\beta$5 creating the five-stranded contiguous sheet (Figure 1B). The structure of DLC2 (Figure 1B) is similar to the structure of DLC1 (Figure 1C). As in DLC1, DLC2 includes a non-prolyl *cis*-peptide bond at Thr-53 [21,22] and additionally a positive $\varphi$ angle is present at Asp-51. The positive $\varphi$ angle at residue Asp-51 reflects its location, together with Pro-52, in a compact turn that links the C-terminus of helix $\alpha$2 to strand $\beta$2. The observation of positive $\varphi$ angles is known to be associated with tight turns in proteins [30]. Backbone angular-order parameters were well defined [$S(\varphi)$ and $S(\psi) \geqslant 0.9$] for residues 7–49, 52, 68, 70–75 and 77–88. The N-terminal 10 residues, including the five cloning artifacts (GPLGS), are disordered in solution and lack any long-range distance constraints.

There are six sequence differences between DLC2 and DLC1 [S2C (where the S is DLC2 and the C is DLC1), D16E, A21S, D23E, M29L and Y41H; Figure 2A]. All are distal from the known ligand-binding site [22] and, with the exception of A21S, are conservative in nature. Tyr-41 is located near the dimer interface although it is not known to be involved in inter-protomer contacts. Ala-21 and Ser-21 are buried and occupy similar positions in the interface between helices $\alpha$1 and $\alpha$2 in both DLC2 and DLC1 respectively. Of the remaining differences, Ser-2 is located in the unstructured N-terminal tail, Asp-16 and Asp-23 together with Met-29 are located on the solvent-exposed face of helix $\alpha$1 in close proximity to Tyr-41 on helix $\alpha$2 (Figure 2B). However, both Met-29 in DLC2 and Leu-29 in DLC1 are largely buried, forming

**Table 1 Structural statistics for the 20 lowest-energy structures of DLC2**

Procheck analysis [35] of Ramachandran regions: numbers in parentheses refer to those residues that have both $\varphi$ and $\psi$ angular order parameters $\geqslant 0.9$. S($\varphi$) and S($\psi$) are the angular order parameters for $\varphi$ and $\psi$. Co-ordinate precision indicates rmsd (root mean square deviation) over backbone (N, C$\alpha$, C′) and all heavy atoms. 5–89 and 5′–89′ refer to residues 5–89 of one protomer and 5′–89′ are the residue numbers of the adjacent protomer in the dimer. $\alpha$1 and $\alpha$2 refer to $\alpha$-helical residues and $\beta$1–$\beta$5 are the $\beta$-strand residues (see Results section). $E_{LJ}$, Lennard–Jones potential.

| Experimental constraints | | |
|---|---|---|
| Total angle and distance constraints (per monomer) | 1602 | |
| Distance constraints: | | |
| Sequential ($\|i-j\|=1$) | 487 | |
| Short range ($1<\|i-j\|<5$) | 285 | |
| Long range ($\|i-j\|\geqslant 5$) | 546 | |
| Hydrogen bonds | 29 | |
| Inter protomer | 99 | |
| Dihedral angles (83 $\varphi$, 44 $\psi$) | 127 | |
| rmsd from experimental distance restraints (Å) | $0.028 \pm 0.001$ | |
| rmsd from experimental dihedral restraints (°) | $0.24 \pm 0.05$ | |
| **rmsd from idealized covalent geometry** | | |
| Bonds (Å) | $0.0075 \pm 0.0001$ | |
| Angles (°) | $0.68 \pm 0.02$ | |
| Impropers (°) | $0.40 \pm 0.02$ | |
| **Measures of structural quality** | | |
| $E_{LJ}$ (kJ · mol$^{-1}$) | $-832 \pm 40$ | |
| Procheck % residues in region of Ramachandran plot [residues with S($\varphi$) and S($\psi$) $\geqslant 0.9$] | | |
| Most favourable | 75.9 (81.6) | |
| Additionally allowed | 21.8 (17.5) | |
| Generously allowed | 1.6 (0.8) | |
| Disallowed | 0.7 (0.1) | |
| Angular order: residues with S($\varphi$) $\geqslant 0.9$ and S($\psi$) $\geqslant 0.9$ | 63/monomer | |
| **Co-ordinate precision** | | |
| Mean pairwise rmsd (Å) | N, C$\alpha$, C | All heavy |
| Dimer | | |
| Residues 5–89, 5′–89′ | $0.96 \pm 0.27$ | $1.78 \pm 0.24$ |
| $\alpha$1, $\alpha$2, $\beta$1–$\beta$5, $\alpha$1′, $\alpha$2′, $\beta$1′–$\beta$5′ | $0.81 \pm 0.26$ | $1.50 \pm 0.19$ |
| Protomer | | |
| Residues 5–89 | $0.67 \pm 0.15$ | $1.59 \pm 0.27$ |
| $\alpha$1, $\alpha$2, $\beta$1–$\beta$5 | $0.50 \pm 0.12$ | $1.30 \pm 0.24$ |

part of the hydrophobic core and therefore exposing only a small percentage of their available surface area to solvent.

### The residues in Bim and Bmf required for binding the DLCs are conserved

The very high sequence identity between DLC1 and DLC2, including residues involved in ligand binding means that the structure itself was insufficient to provide information on binding specificity. Site-directed mutagenesis of residues within the LBDs of $Bim_L$ and Bmf (Figure 3A), which were required for binding DLC1 and DLC2 (Figure 3B), was used to characterize the nature of this interaction. A series of single and double mutants across the binding site shows the essential nature of Gln-55 in $Bim_L$ and its equivalent, Gln-71, in Bmf (Figure 3B). Mutation of the preceding threonine also reduces binding of both Bim and Bmf to their respective DLCs. The binding domains we have mapped for Bim and Bmf are in agreement with earlier studies on $Bim_L$ [13,14]. In the crystal structure of the DLC1/nNOS–LBD peptide complex [22], Gln-234 of nNOS, the equivalent residue of Gln-55 and Gln-71 in $Bim_L$ and Bmf respectively, makes cross-dimer contacts with Ile-34 via hydrophobic interactions and contacts Glu-35 and Lys-36 via hydrogen-bond interactions between side chains. Other mutations have less impact. For example, mutation of Asp-51 or Thr-56 alone in $Bim_L$ was not sufficient to abolish binding (Figure 3B) but the double mutant D51A/T56A greatly diminished binding.

### Binding of LBD peptides induces similar changes in DLC1 and DLC2

To further characterize the interaction between Bmf and DLC2, the solution properties of a complex (formed with Bmf–LBD residues 64–80, SQEDKATQTLSPASPSQ) was investigated using NMR. Tight binding of Bmf–LBD to DLC2 was demonstrated by its ability to compete with BmfΔC25 for DLC2 binding (results not shown). At sub-stoichiometric amounts of Bmf peptide, more than two sets of resonances were observed; of these, one set was from the free DLC2, another was from the complexed form (indicating the complexes are in slow exchange on the NMR time scale) and the remaining resonances were from the non-symmetrical partially complexed DLC2 dimer. Addition of two equivalents of Bmf–LBD to DLC2 generated a single set of resonances in the $^1$H-/$^{15}$N-HSQC spectrum. These data, in conjunction with results from size-exclusion chromatography, suggest that a tightly bound symmetrical dimer of dimers ([DLC2–peptide]$_2$) forms when stoichiometric amounts of Bmf–LBD peptide are added. Furthermore, the $^1$H-/$^{15}$N-HSQC spectrum for DLC2, in the presence and absence of Bmf–LBD, revealed that the largest chemical shift changes on ligand binding occur for residues located in the $\beta$3–$\beta$4 region of DLC2 and smaller changes are observed in $\alpha$2 and $\beta$2 [22] (Figure 3C). Residues located in these regions form part of the LBD-binding interface. Comparison of similar ligand-binding studies using Bim peptides and DLC1 suggests that Bim and Bmf–LBD peptides bind DLC1 and DLC2 in a similar way (Figure 3C).

### The determinants of specific binding for DLC1 or DLC2 are not present in Bim or Bmf

When isolated from cells Bmf is found to only associate with DLC2, while Bim is primarily found in association with DLC1, yet the studies with peptides suggest that the binding sites are highly conserved. Binding studies using purified recombinant $Bim_L$ΔC27 and BmfΔC25 also indicated that the binding sites are equivalent since both proteins could bind DLC1 and DLC2 (Figure 4A). Indeed, when Bim and Bmf were added together with either DLC1 or DLC2 preferential binding was not observed (Figure 4A, lanes 5 and 6). Although hydrophobic C-terminal residues are missing from the recombinant forms of Bim and Bmf used here, this experiment suggests that sequences outside of their LBDs do not confer the binding specificity.

The identity of the LBD binding sites was further demonstrated by mutagenesis of the DLCs. Some of the residues, identified by NMR as the binding region of $Bim_L$ peptide on DLC1, namely Glu-35, Thr-67, His-68 and Phe-73 [13] were mutated to Ala in DLC1 and DLC2. Mutations of Thr-67 or Phe-73 in DLC1 almost completely abrogated binding to both $Bim_L$ΔC27 and BmfΔC25 (Figure 4B), emphasizing the similarity in the interactions between DLC1 and $Bim_L$ or Bmf. Likewise, the disruptive

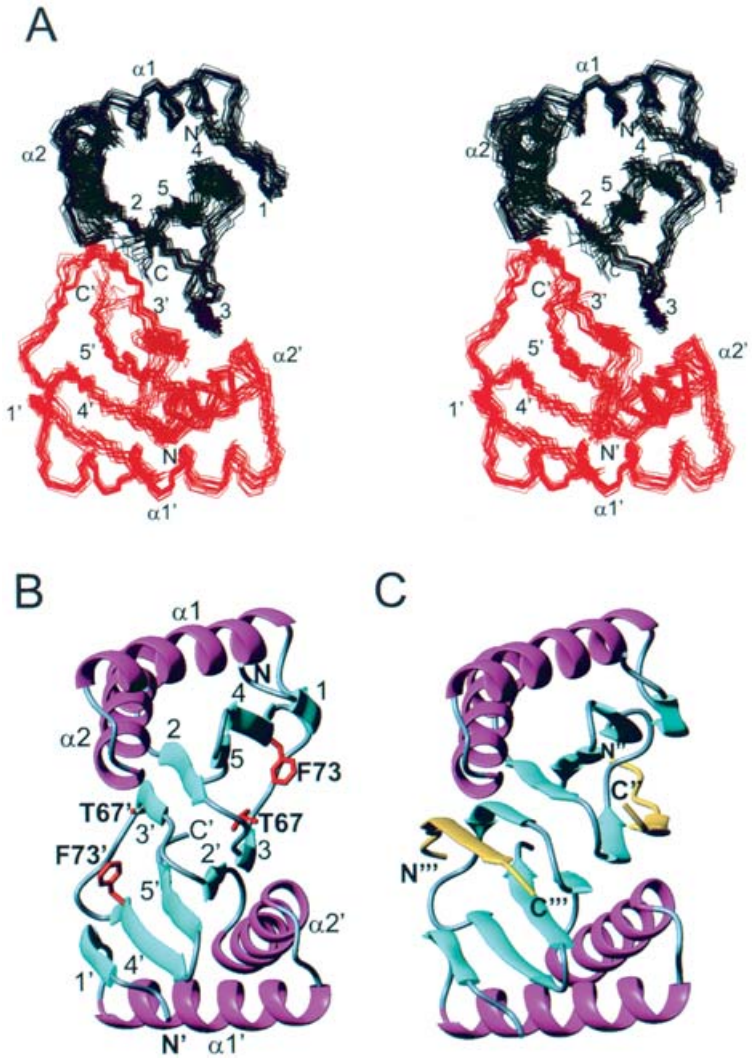


**Figure 1 Structure of DLC2**

(**A**) Stereo view of the family of 20 structures of DLC2 superimposed over the backbone atoms (N, C$\alpha$, C′) of residues 5–89. Residues 5–89 are shown and one subunit is coloured orange. $\beta$-Strands are labelled 1–5 and $\alpha$-helices $\alpha$1 and $\alpha$2 are also shown; on the adjacent subunit $\beta$-strands 1′–5′ and $\alpha$-helices $\alpha$1′ and $\alpha$2′ are shown. (**B**) Ribbon diagram of the structure closest to the mean for DLC2. The secondary structure of each monomer subunit consists of two $\alpha$-helices, $\alpha$1 (residues 15–31) and $\alpha$2 (35–49) and five $\beta$-strands, 1–5 ($\beta$1, 8–12; $\beta$2, 54–59; $\beta$3, 63–66; $\beta$4, 72–78; $\beta$5, 82–87; strands are numbered according to the DLC1–nNOS crystal structure [22]). Four of these strands, $\beta$1, $\beta$2, $\beta$4 and $\beta$5, form an extended sheet with $\beta$3′ from the adjacent monomer. A bulge (residues 8–11) is present in $\beta$1. Side-chains are shown for Thr-67 and Phe-73, key determinates of ligand binding. (**C**) Backbone ribbon of DLC1 (LC8) bound to nNOS peptide (yellow; PDB code 1CMI [22]).

mutations T67A and F73A in DLC2 also reduced binding of both $Bim_L$ and Bmf. Surprisingly, mutation of Glu-35 in DLC1 does not appear to affect binding, although this residue contacts the highly conserved glutamine (Glu-55 in $Bim_L$ and Glu-71 in Bmf). Likewise, the mutation H68A has little effect on the binding of $Bim_L$ or Bmf. In the published structures His-68 contacts the main chain and the less highly conserved Thr-231 of nNOS (Lys-52 of $Bim_L$, Lys-68 of Bmf), and this may account for the tolerance at this position.

When a reverse two-hybrid screen of 5000 mutated clones was carried out to search for residues in DLC1, besides Phe-73 and Thr-67, that are required for binding to $Bim_L$ [5–7], Tyr-75 and Phe-76 were found to be disruptive (Figure 4C). These two residues are in close proximity to the identified binding site and suggest that the contacts required for complex formation are confined to this region. Collectively, these data demonstrate that the binding sites within DLC1 and DLC2 are conserved and that recombinant Bim and Bmf cannot discriminate between these two proteins. In cells the specific compartmentalization of these proteins is probably mediated by other protein components that results in specific binding of DLC1 to Bim, and DLC2 to Bmf.

### Mapping the interaction of DLC1 and DLC2 with their respective dynein and myosin V motor complexes

When isolated from cells DLC1 co-purifies with the dynein motor-enriched fraction, whereas DLC2 purifies mainly with the myosin V motor [9] (Figure 5). To investigate how this specificity might be defined, we swapped residues that differ between DLC1 and DLC2. Interestingly, replacement of the most divergent surface residue in DLC1 (His-41), with the corresponding residue in DLC2 (Tyr), significantly abrogated its localization with the dynein motor (Figure 5A). The corresponding mutation in DLC2 (replacing Tyr-41 with His) displaces DLC2 from the myosin

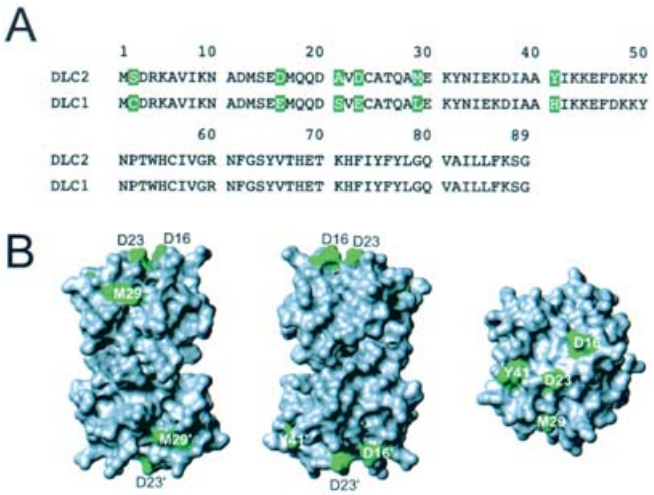


**Figure 2 Sequence differences in DLCs map to the surface**

(**A**) Alignment of the sequences for DLC1 and DLC2 (shading indicates the differences). (**B**) Surface diagram highlighting the residues (green) that differ between DLC2 and DLC1, using the structure of DLC2 (residues 5–89). The left-hand view is the same molecular orientation as the ribbon in Figure 1(B), the middle view a 180° rotation about the vertical axis and the right-hand view is a 90° rotation about the horizontal axis.

V motor whereas mutations to other surface residues that differ between the two molecules had no impact (Figure 5B). Thus, His-41 of DLC1 and Tyr-41 of DLC2 probably make critical contacts that are responsible for bringing these polypeptides to the dynein and myosin V motors respectively.

## DISCUSSION

One of the main objectives of these studies was to elucidate the mechanism behind the *in vivo* specificity shown by DLC2 for the pro-apoptotic BH3-only protein Bmf. The solution structure of DLC2 was found to be well defined, with the exception of a few N-terminal residues that lack long-range constraints (Figure 1). Two well-ordered monomers form a symmetrical dimer that is created by sharing of a strand from the adjacent subunit (Figure 1). DLC2 has the greatest structural similarity to the crystal structure of the DLC1–nNOS complex (PDB code 1CMI) [22] with a rmsd (root mean square deviation) of 1.34 Å when superimposed over the backbone (N, C$\alpha$, C′) of residues 5–89 of the dimer. The same superimposition with the NMR-determined structure of apo-DLC1 (PDB code 1F3C) [13] gives a rmsd of 2.70 Å. Similarly, the NMR structures of DLC1 bound to $Bim_L$ (PDB code 1F95) or nNOS (PDB code 1F96) peptides have rmsd values of 1.77 and 1.49 Å respectively when compared with that of DLC2.

The majority of sequence differences between DLC2 and DLC1 (Figure 2A) map to a distinct surface on DLC2 (Figure 2B), which is remote from the LBD-binding site and therefore precluded from having any direct involvement in ligand binding. Moreover, identical residues on DLC1 and DLC2 form the LBD-binding site and the LBD peptides bind in a groove formed between helix $\alpha$2 of one monomer and the third and fourth $\beta$-strands of the other monomer (Figure 1B), with hydrophobic residues projecting from the $\beta$-strands forming a hydrophobic surface for peptide binding. In the DLC1/nNOS–LBD and DLC1/$Bim_L$–LBD structures the LBD peptide forms an anti-parallel strand adjacent to the third $\beta$-strand of DLC1 [21,22], extending the $\beta$-sheet. The hydrophobic side chains projecting from the peptide strand form hydrophobic contacts with residues in the groove. One of the residues within both DLC1 and DLC2 whose mutation abrogates peptide binding, F73A, lies on strand $\beta$4 and forms part of this hydrophobic pocket while the other residue shown to be required for binding, Thr-67, is located in the $\beta$3–$\beta$4 binding region. Thr-67 in DLC1 makes hydrogen bonds with Asp-51 in $Bim_L$ [21] and Asp-230 in nNOS–LBD [22]. Asp-67 in Bmf would be expected to fulfil this role although, as seen for $Bim_L$, mutation of this residue to alanine only results in a slight decrease in binding (Figure 3B). Surprisingly, mutation of Glu-35 in DLC1 does not disrupt binding to either $Bim_L$ or Bmf, although in both published complex structures [21,22] this residue interacts with the highly conserved glutamine that is required for binding (Figure 3B).

Analysis of the Bmf–LBD mutants suggests that cells may be sensitive to small amounts of free Bmf. The mutants D67G/K68A/T70A and A69P reduced survival in FDC-P1 cells exposed to apoptotic stimuli and the same mutations abrogate DLC2 binding *in vivo* [9]. However, both mutants still showed some residual DLC2 binding *in vitro* (Figure 3B). Mutation of Ala-69 to proline, but not to aspartic acid, in recombinant Bmf disrupted binding (Figure 3B), suggesting that the side chain does not make important contacts but instead proline distorts the conformation of the main chain to reduce binding.

The pattern of chemical shift changes in $^{1}H$-/$^{15}N$-HSQC spectra, induced upon binding of Bmf–LBD to DLC2, are similar to those we observed for DLC1 and those reported by Zhang and co-workers [41], when an equivalent peptide from $Bim_L$ (Bim–LBD) was bound (Figure 3C). In addition the changes in $^{1}H$-/$^{15}N$-HSQC spectra of DLC1 when Bmf–LBD peptide is titrated into $^{15}N$-labelled DLC1 protein are similar to those observed when Bim-LBD is added to the same protein (results not shown). Furthermore, NOEs observed during the current studies, in the $^{15}N$- and $^{13}C$-edited NOESY spectra of DLC2/Bmf–LBD and DLC1/Bim–LBD show essentially identical patterns, and these, coupled with the chemical shift changes (Figure 3C) indicate that both LBDs interact in a similar manner with their respective DLCs. In conjunction with the mutational mapping analysis and the high level of sequence identity (93 %) between DLC1 and DLC2, our data suggest that Bmf binds to DLC2 in an extended conformation, adjacent to $\beta$3, and analogous to that seen for $Bim_L$ and nNOS peptides bound to DLC1 [21,22]. These short $Bim_L$ and Bmf LBDs are shown in Figure 3(A) and the sequence motif XKXTQT is consistent with many other DLC-binding sequences [13,42].

It has been observed that, *in vivo*, Bmf is found to associate only with DLC2 [9] whereas $Bim_L$ is associated mostly with DLC1 [8]. Neither the short LBD sequence motif alone nor the structures of the DLCs explains this specific localization. The small number of differences between the DLCs are confined to solvent-exposed regions remote from the LBD-binding surface that do not appear to make direct contact with the ligand (Figure 2B). Additionally, residues outside the short binding domain on $Bim_L$ and Bmf do not apparently confer this specificity. Both $Bim_L\Delta C27$ and Bmf$\Delta$C25 (two recombinant molecules with their putative membrane-binding domains truncated) bind either DLC1 or DLC2 and can be competitively displaced by the other ligand (Figure 4A). These results suggest that other components within the cell must interact with the DLC complexes and confer specific binding.

In the assembled motor complexes, it is likely that a given DLC dimer binds to two different molecules. It has been proposed that one site is loaded with the cargo, while the other binds a component of the motor complex. For instance, DLCs are known to bind IC74, the dynein intermediate chain [9,13,43], and the recognition sequence in IC74 suggests that binding to DLC occurs in a similar manner as seen for $Bim_L$ and nNOS [13]. As in the case of

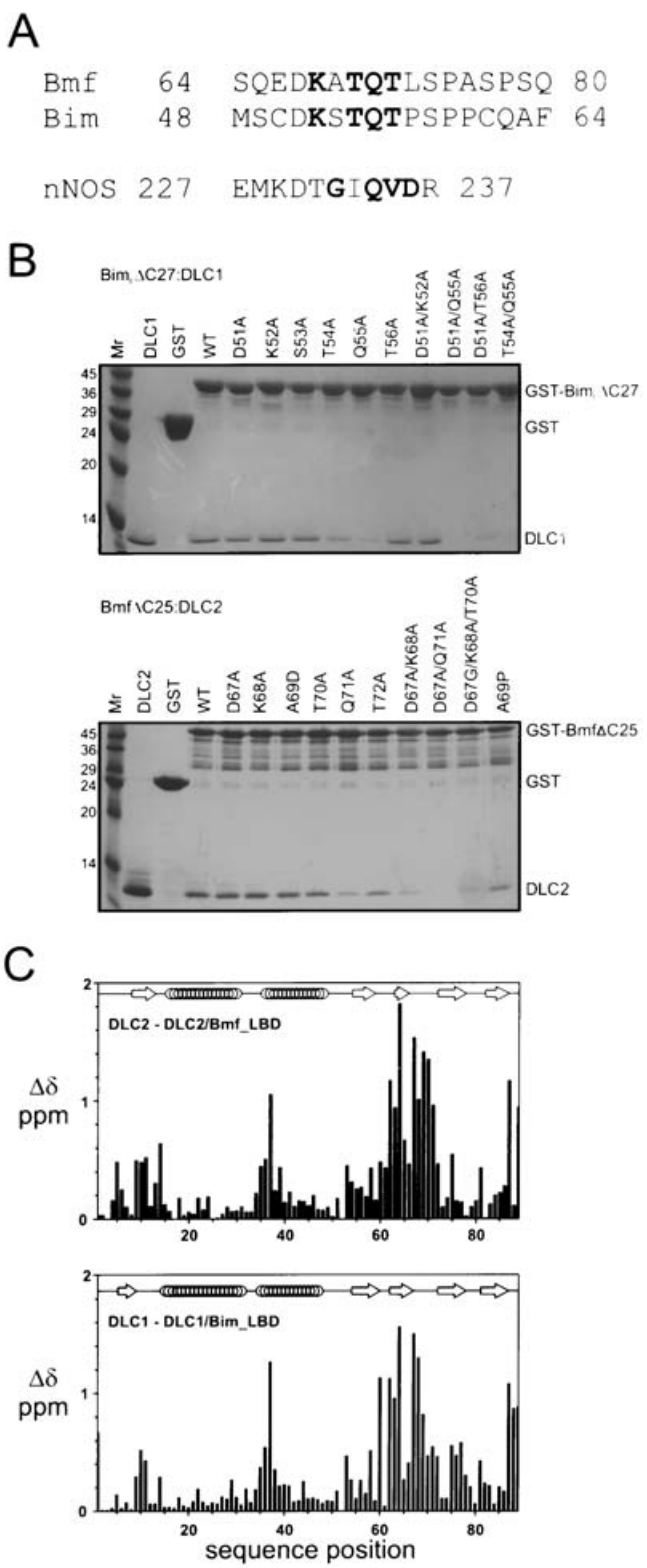


**Figure 3 Identification of the interaction interfaces**

(**A**) LBD sequence motifs for Bim$_L$ and Bmf. Residues in bold are those that are conserved over a range of DLC-binding proteins [13,14]. For reference, the nNOS peptide is shown with residues that correspond to the second conserved binding motif highlighted in bold. (**B**) Mutagenesis of the LBDs within Bim and Bmf. Purified GST fusion proteins of Bim$_L$ΔC27 and BmfΔC25 were expressed and purified as described in the text. Approximately equivalent amounts of the resin-bound GST fusion proteins were mixed with soluble DLC1 or DLC2 as indicated. Gels were stained with Coomassie Blue. The intensity of the band corresponding to the soluble protein was used to estimate the relative strength of binding. The lanes are labelled according to the mutation, WT corresponds to wild-type Bim or Bmf. Mr refers to the molecular-mass markers indicated in kDa. (**C**) Histogram showing the chemical shift differences between amide resonances of free and bound DLC complexes induced by ligand binding. Chemical shift differences between DLC2 – DLC2/Bmf-LBD and DLC1 – DLC1/Bim-LBD are plotted as weighted average chemical shift differences to take account of both $^1$H and $^{15}$N resonance perturbations according to the equation $\Delta\delta = [\Delta\delta^2_{HN} + 0.17\Delta\delta^2_{15N}]^{1/2}$ where $\Delta\delta_{HN}$ and $\Delta\delta_{15N}$ are the chemical shift changes of the HN and N resonances on binding ligand respectively [44]. The position of the secondary structure elements indicated for DLC1 are from Liang et al. [22] and those for DLC2 are as determined in this study.

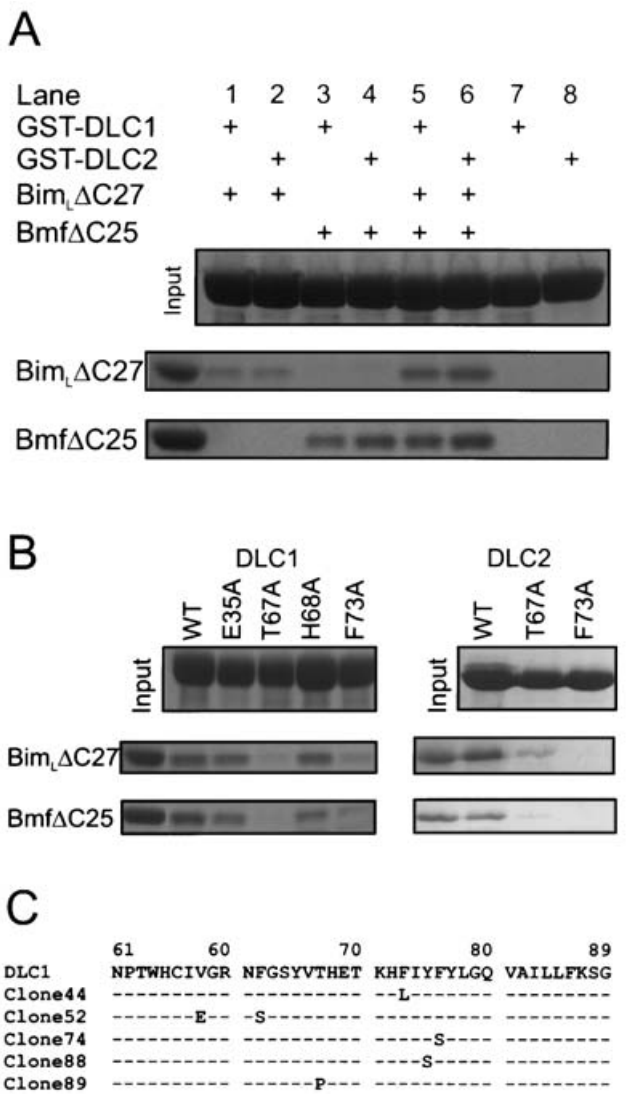


**Figure 4 Bim and Bmf can both bind to DLC1 and DLC2 *in vitro***

(**A**) The ability of DLC1 and DLC2 to discriminate between Bim and Bmf was assessed. Soluble Bim$_L$ΔC27 and BmfΔC25 were mixed with resin bound GST-DLC1 and GST-DLC2 in isolation (lanes 1–4) or together (lanes 5 and 6). Samples were analysed as described for Figure 3(A). (**B**) Identification of residues required for binding Bim or Bmf within the DLC binding groove. Experiments were carried out as in Figure 3(A) except in this instance the GST–DLC was attached to the resin and soluble Bim$_L$ΔC27 or BmfΔC25 was added. The lanes are labelled according to the site of the mutated residue on DLC1 or DLC2. For example, E35A corresponds to GST-DLC1 (E35A). WT, wild type. (**C**) Alignment of the sequences corresponding to the five clones obtained using the reverse yeast two-hybrid screen. The differences relative to wild-type DLC1 are indicated. Clone 44 and clone 52 also had D37V and V22A mutations respectively.

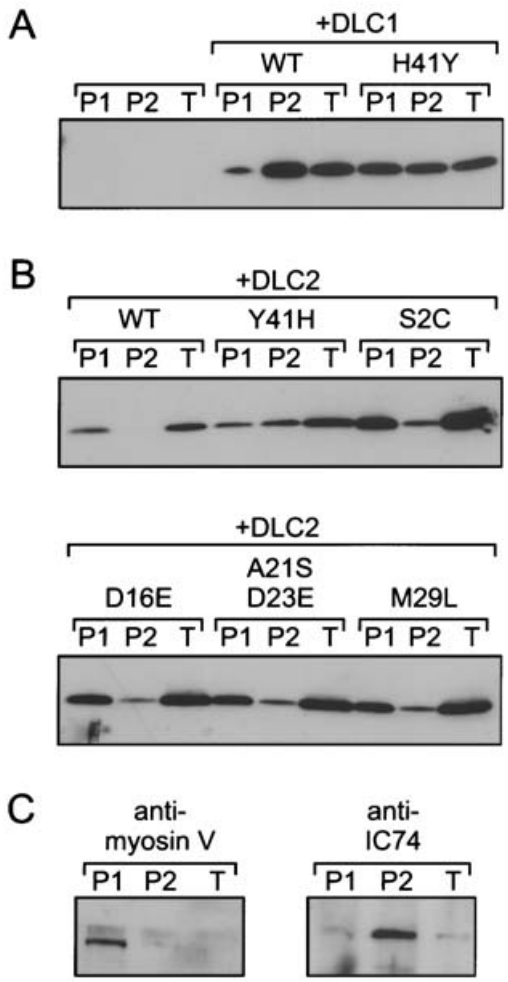


**Figure 5 Localization of DLC1 and DLC2 is primarily determined by residue 41**

(**A**) His-41 of DLC1 promotes its interaction with the dynein motor complex. Parental HEK-293T cells or those transiently expressing FLAG-tagged wild-type or the H41Y mutant DLC1 were fractionated into P1 (myosin V motor-enriched) and P2 (dynein motor-enriched) fractions. (**B**) Tyr-41 of DLC2, but not the other residues that differ from DLC1, promotes DLC2 binding to the myosin V motor complex. HEK-293T cells expressing FLAG-tagged wild-type or mutant forms of DLC2 were fractionated as in (**A**). Equivalent P1 and P2 fractions, and total cell lysate before fractionation (T), were probed with the anti-FLAG M2 monoclonal antibody. WT refers to wild-type DLC1 or DLC2. (**C**) Confirming purity of the myosin V (P1) or dynein (P2) motor-enriched fractions. Equivalent HEK-293T lysates fractionated (as described in the Experimental section) were probed with antibodies recognizing anti-myosin V (left) or an anti-(dynein intermediate chain) (anti-IC74; right). Unlike myosin V or dynein intermediate chain IC74, FLAG-tagged DLC1 or DLC2 was readily detected in the total cell lysate because these proteins were overexpressed.

many multiprotein complexes, we expect the nature of the first protein bound would influence those that can bind at the second site. The exact mechanism by which this could arise, like other systems, requires a detailed analysis of the kinetics and thermodynamics of the protein–protein interactions, preferably using complexes of full-length proteins. To date, all binding and structural studies have used purified DLCs that have the same molecule bound in both binding sites.

How do DLC1 and DLC2 compartmentalize to the dynein- and myosin V-based motors respectively? As most of the differences between DLC1 and DLC2 mapped on to their surfaces (Figure 2B), we speculated that some of these differences may allow their unique localization within cells. Indeed, replacing His-41 in DLC1 with tyrosine (residue 41 in DLC2) appears to divert DLC1 away from the dynein to the myosin V motor complex (Figure 5A). As expected, the complementary mutation in DLC2 changed its location to the dynein motor (Figure 5B). Thus mutational studies suggest that residue 41 (histidine in DLC1 and tyrosine in DLC2) is responsible for the specific localization of DLC1 and DLC2 in mammalian cells. However, the direct target for their binding at these locations is currently not known.

We have established that the 3D structures of DLC2 and DLC1 are essentially identical, yet their 'BH3-only' partners, $Bim_L$ and Bmf, are found associated in a specific manner in cells. $Bim_L$ and Bmf have equal avidity for either DLC, suggesting that the elements required for specific binding to their respective DLCs lie outside these proteins, although a role for the C-terminal residues cannot be excluded. The DLCs are in turn sequestered to particular cellular compartments and as a result their ligand preference may be determined by other components of their compartment. A molecular basis for the specific sequestration of DLC1 and DLC2, to their dynein and myosin V motors respectively, is provided by our demonstration that residue 41 plays a critical role in determining their location. This suggests that a molecular surface centred on residue 41 may make contacts with other components of their respective motor complexes, ensuring the specificity of their compartmentalization. Given their conserved sequence, structural and ligand-binding characteristics it is remarkable that the DLCs specifically compartmentalize their ligands.

We thank Jerry Adams and Suzanne Cory for reagents and encouragement. This work was supported by fellowships and grants from the Marsden Fund (New Zealand), NHMRC (Australia; 257502), the United States NCI (CA 80188), the Leukemia and Lymphoma Society (Specialized Center of Research; 7015-02), the Cancer Council of Victoria and the Dr Josef Steiner Cancer Research and Sylvia & Charles Viertel Charitable Foundations.

## REFERENCES

1 Bouillet, P., Metcalf, D., Huang, D. C., Tarlinton, D. M., Kay, T. W., Kontgen, F., Adams, J. M. and Strasser, A. (1999) Proapoptotic Bcl-2 relative Bim required for certain apoptotic responses, leukocyte homeostasis, and to preclude autoimmunity. Science **286**, 1735–1738
2 Bouillet, P., Purton, J. F., Godfrey, D. I., Zhang, L. C., Coultas, L., Puthalakath, H., Pellegrini, M., Cory, S., Adams, J. M. and Strasser, A. (2002) BH3-only Bcl-2 family member Bim is required for apoptosis of autoreactive thymocytes. Nature (London) **415**, 922–926
3 Huang, D. C. and Strasser, A. (2000) BH3-only proteins-essential initiators of apoptotic cell death. Cell **103**, 839–842
4 Puthalakath, H. and Strasser, A. (2002) Keeping killers on a tight leash: transcriptional and post-translational control of the pro-apoptotic activity of BH3-only proteins. Cell Death Differ. **9**, 505–512
5 Oda, E., Ohki, R., Murasawa, H., Nemoto, J., Shibue, T., Yamashita, T., Tokino, T., Taniguchi, T. and Tanaka, N. (2000) Noxa, a BH3-only member of the Bcl-2 family and candidate mediator of p53-induced apoptosis. Science **288**, 1053–1038
6 Nakano, K. and Vousden, K. H. (2001) PUMA, a novel proapoptotic gene, is induced by p53. Mol. Cell **7**, 683–694
7 Yu, J., Zhang, L., Hwang, P. M., Kinzler, K. W. and Vogelstein, B. (2001) PUMA induces the rapid apoptosis of colorectal cancer cells. Mol. Cell **7**, 673–682
8 Puthalakath, H., Huang, D. C., O'Reilly, L. A., King, S. M. and Strasser, A. (1999) The proapoptotic activity of the Bcl-2 family member Bim is regulated by interaction with the dynein motor complex. Mol. Cell **3**, 287–296
9 Puthalakath, H., Villunger, A., O'Reilly, L. A., Beaumont, J. G., Coultas, L., Cheney, R. E., Huang, D. C. and Strasser, A. (2001) Bmf: a proapoptotic BH3-only protein regulated by interaction with the myosin V actin motor complex, activated by anoikis. Science **293**, 1829–1832
10 King, S. M. (2000) The dynein microtubule motor. Biochim. Biophys. Acta **1496**, 60–75
11 Adams, J. M. and Cory, S. (1998) The Bcl-2 protein family: arbiters of cell survival. Science **281**, 1322–1326
12 Lei, K. and Davis, R. J. (2003) JNK phosphorylation of Bim-related members of the Bcl2 family induces Bax-dependent apoptosis. Proc. Natl. Acad. Sci. U.S.A. **100**, 2432–2437

13 Lo, K. W., Naisbitt, S., Fan, J. S., Sheng, M. and Zhang, M. (2001) The 8-kDa dynein light chain binds to its targets via a conserved (K/R)XTQT motif. J. Biol. Chem. **276**, 14059–14066
14 Rodriguez-Crespo, I., Yelamos, B., Roncal, F., Albar, J. P., Ortiz de Montellano, P. R. and Gavilanes, F. (2001) Identification of novel cellular proteins that bind to the LC8 dynein light chain using a pepscan technique. FEBS Lett. **503**, 135–141
15 Epstein, E., Sela-Brown, A., Ringel, I., Kilav, R., King, S. M., Benashski, S. E., Yisraeli, J. K., Silver, J. and Naveh-Many, T. (2000) Dynein light chain binding to a 3′-untranslated sequence mediates parathyroid hormone mRNA association with microtubules. J. Clin. Invest. **105**, 505–512
16 Hirokawa, N. (1998) Kinesin and dynein superfamily proteins and the mechanism of organelle transport. Science **279**, 519–526
17 Raux, H., Flamand, A. and Blondel, D. (2000) Interaction of the rabies virus P protein with the LC8 dynein light chain. J. Virol. **74**, 10212–10216
18 Jacob, Y., Badrane, H., Ceccaldi, P. E. and Tordo, N. (2000) Cytoplasmic dynein LC8 interacts with lyssavirus phosphoprotein. J. Virol. **74**, 10217–10222
19 Sodeik, B., Ebersold, M. W. and Helenius, A. (1997) Microtubule-mediated transport of incoming herpes simplex virus 1 capsids to the nucleus. J. Cell Biol. **136**, 1007–1021
20 Tochio, H., Ohki, S., Zhang, Q., Li, M. and Zhang, M. (1998) Solution structure of a protein inhibitor of neuronal nitric oxide synthase. Nat. Struct. Biol. **5**, 965–969
21 Fan, J.-S., Zhang, Q., Tochio, H., Li, M. and Zhang, M. (2001) Structural basis of diverse sequence-dependent target recognition by the 8 kDa dynein light chain. J. Mol. Biol. **306**, 97–108
22 Liang, J., Jaffrey, S. R., Guo, W., Snyder, S. H. and Clardy, J. (1999) Structure of the PIN/LC8 dimer with a bound peptide. Nat. Struct. Biol. **6**, 735–740
23 Day, C. L., Dupont, C., Lackmann, M., Vaux, D. L. and Hinds, M. G. (1999) Solution structure and mutagenesis of the caspase recruitment domain (CARD) from Apaf-1. Cell Death Differ. **6**, 1125–1132
24 Duttweiler, H. M. (1996) A highly sensitive and non-lethal beta-galactosidase plate assay for yeast. Trends Genet. **12**, 340–341
25 Wach, A., Brachat, A., Pohlmann, R. and Philippsen, P. (1994) New heterologous modules for classical or PCR-based gene disruptions in *Saccharomyces cerevisiae*. Yeast **10**, 1793–1808
26 Sattler, M., Schleucher, J. and Griesinger, C. (1999) Heteronuclear multidimensional NMR experiments for the structure determination of proteins in solution employing pulsed field gradients. Prog. Nucl. Magn. Reson. Spectrosc. **34**, 93–158
27 Hwang, T. L., van Zijl, P. C. and Mori, S. (1998) Accurate quantitation of water-amide proton exchange rates using the phase-modulated CLEAN chemical EXchange (CLEANEX-PM) approach with a Fast-HSQC (FHSQC) detection scheme. J. Biomol. NMR **11**, 221–226
28 Bartels, C., Xia, T. H., Billeter, M., Güntert, P. and Wüthrich, K. (1995) The program XEASY for computer-supported NMR spectral analysis of biological macromolecules. J. Biomol. NMR **6**, 1–10
29 Luginbühl, P., Szyperski, T. and Wüthrich, K. (1995) Statistical basis for the use of $^{13}C^{\alpha}$ chemical-shifts in protein structure determination. J. Magn. Reson. Ser. B **109**, 229–233
30 Ludvigsen, S. and Poulsen, F. M. (1992) Positive $\varphi$-angles in proteins by nuclear magnetic resonance spectroscopy. J. Biomol. NMR **2**, 227–233
31 O'Donoghue, S. I., King, G. F. and Nilges, M. (1996) Calculation of symmetric multimer structures from NMR data using *a priori* knowledge of the monomer structure, co-monomer restraints, and interface mapping: The case of leucine zippers. J. Biomol. NMR **8**, 193–206
32 Güntert, P., Mumenthaler, C. and Wüthrich, K. (1997) Torsion angle dynamics for NMR structure calculation with the new program DYANA. J. Mol. Biol. **273**, 283–298
33 Brünger, A. T., Adams, P. D., Clore, G. M., DeLano, W. L., Gros, P., Grosse-Kunstleve, R. W., Jiang, J. S., Kuszewski, J., Nilges, M., Pannu, N. S. et al. (1998) Crystallography & NMR system: A new software suite for macromolecular structure determination. Acta Crystallogr. D Biol. Crystallogr. **54**, 905–921
34 Linge, J. P. and Nilges, M. (1999) Influence of non-bonded parameters on the quality of NMR structures: A new force field for NMR structure calculation. J. Biomol. NMR **13**, 51–59
35 Laskowski, R. A., Rullmann, J. A. C., MacArthur, M. W., Kaptein, R. and Thornton, J. M. (1996) AQUA and PROCHECK-NMR: Programs for checking the quality of protein structures solved by NMR. J. Biomol. NMR **8**, 477–486
36 Koradi, R., Billeter, M. and Wüthrich, K. (1996) MOLMOL: a program for display and analysis of macromolecular structures. J. Mol. Graph. **14**, 51–55
37 Huang, D. C., Adams, J. M. and Cory, S. (1998) The conserved N-terminal BH4 domain of Bcl-2 homologues is essential for inhibition of apoptosis and interaction with CED-4. EMBO J. **17**, 1029–1039
38 O'Connor, L., Strasser, A., O'Reilly, L. A., Hausmann, G., Adams, J. M., Cory, S. and Huang, D. C. (1998) Bim: a novel member of the Bcl-2 family that promotes apoptosis. EMBO J. **17**, 384–395
39 Espreafico, E. M., Cheney, R. E., Matteoli, M., Nascimento, A. A., De Camilli, P. V., Larson, R. E. and Mooseker, M. S. (1992) Primary structure and cellular localization of chicken brain myosin-V (p190), an unconventional myosin with calmodulin light chains. J. Cell Biol. **119**, 1541–1557
40 Paschal, B. M., Shpetner, H. S. and Vallee, R. B. (1991) Purification of brain cytoplasmic dynein and characterization of its *in vitro* properties. Methods Enzymol. **196**, 181–191
41 Fan, J. S., Zhang, Q., Li, M., Tochio, H., Yamazaki, T., Shimizu, M. and Zhang, M. (1998) Protein inhibitor of neuronal nitric-oxide synthase, PIN, binds to a 17-amino acid residue fragment of the enzyme. J. Biol. Chem. **273**, 33472–33481
42 Fan, J. S., Zhang, Q., Tochio, H. and Zhang, M. (2002) Backbone dynamics of the 8 kDa dynein light chain dimer reveals molecular basis of the protein's functional diversity. J. Biomol. NMR **23**, 103–114
43 Makokha, M., Hare, M., Li, M., Hays, T. and Barbar, E. (2002) Interactions of cytoplasmic dynein light chains Tctex-1 and LC8 with the intermediate chain IC74. Biochemistry **41**, 4302–4311
44 Farmer, B. T., Constantine, K. L., Goldfarb, V., Friedrichs, M. S., Wittekind, M., Yanchunas, Jr, J., Robertson, J. G. and Mueller, L. (1996) Localizing the $NADP^{+}$ binding site on the MurB enzyme by NMR. Nat. Struct. Biol. **3**, 995–997

Received 15 August 2003/10 October 2003; accepted 15 October 2003
Published as BJ Immediate Publication 15 October 2003, DOI 10.1042/BJ20031251